A Laser-Activated MEMS Transducer for Efficient Generation of Narrowband Longitudinal Ultrasonic Waves

Xuesheng Chen, Theodosia Stratoudaki, Steve D. Sharples, and Matt Clark

***Abstract*—In this paper, we demonstrate an optically powered microelectromechanical system (MEMS) transducer. It was designed and fabricated using MEMS techniques, and can generate narrowband ultrasonic bulk waves from a broadband laser excitation pulse with high efficiency. The transducer is a two-mask-level MEMS device with a microdisk seated on a microstem. When a laser pulse is incident on the disk center, a resonant flapping motion of the disk is actuated because of the thermomechanical interaction between the absorbing and non-absorbing parts of the disk, coupling a narrowband longitudinal bulk wave propagating along the axis of the stem into the sample. Finite element (FE) methods were used to simulate the generated ultrasound; the results agree well with experimental measurements. Experiments with the fabricated transducers have shown that narrowband ultrasound with a high SNR/amplitude was generated successfully; compared with normal thermoelastic generation, ultrasound with at least 5 times higher amplitude can be achieved by an optimized MEMS transducer. The transducer is inexpensive, compact, and simple to use.**

I. Introduction

Laser-based ultrasonic techniques have received much attention in recent decades because laser ultrasonic inspection has advantages over traditional ultrasound generation and detection that are based on contact techniques. The ability to operate remotely from the sample surface makes noncontact, couplant-free online generation and detection of ultrasound possible, allowing inspection of areas where access is difficult. However, compared with conventional ultrasound techniques, the SNR of laser ultrasound is low because of the shot noise of optical detection. Raising the power of the laser pulse to produce ultrasound with a higher amplitude is one of the solutions; however this is constrained by the damage limit [1]. Great efforts have been made to overcome this drawback in the last two decades by either increasing the amplitude of the laser ultrasound, strengthening the detection sensitivity, or both [2]–[4].

To remotely generate and detect laser ultrasound, different complex and expensive systems have been developed (as reviewed in [2]) such as confocal Fabry-Pérot interferometers, photo-EMF detectors, electromagnetic acoustic transducers, and knife-edge detectors [5]. This also led to the development of hybrid ultrasonic systems [3]. For detection of ultrasound with high sensitivity, a cantilever optical MEMS detection transducer with a sensitivity a few hundred times higher than that of the conventional methods has also been reported recently [4].

To increase the amplitude of laser-generated ultrasound, different techniques have been successfully developed. One technique is to deposit a layer of material, such as graphite, with a higher optical absorption coefficient onto the surface of a sample [6]. This can effectively increase the absorbed optical energy. In [7], laser light was line-focused so that the optical power can be effectively increased while keeping the power density of the laser pulse within the nondestructive range. By combining the techniques in [6] and [7], generation transducers with patterned absorption layers have also been developed [8], this can be applied to generate narrowband ultrasound with improved SNR. A different technique is to achieve higher amplitude by narrowing the bandwidth. When the optical power density is constrained, it concentrates the ultrasound within a narrower bandwidth. This has been done by different methods, for instance different lasers have been used to generate narrowband laser ultrasound [9], [10].

In addition to these methods, complex optical arrays [11], [12], special methods [13], and optical transducer systems [8] were also developed for the generation of narrowband ultrasound with higher amplitude/SNR.

In this paper, we presented an optically powered MEMS transducer for the generation of narrowband ultrasound with high amplitude/SNR, providing a different solution to the optical shot noise problem for laser ultrasound generation and detection. It is a 3-D elastomechanical microstructure, a typical MEMS device, consisting of a resonant microdisk, seated on a solid microstem, as shown in Fig. 1(a). This transducer generates longitudinal waves in a narrow bandwidth with higher amplitude than would be excited using the same optical power without the transducer present. It also has high efficiency, compact size, and a wide application range by using simple optics with a common pulsed laser source.

II. Working Principle

A. Resonant Flapping Motion of the Microdisk and its Frequency

In normal thermoelastic excitation in which a laser pulse is incident on the surface of a sample, the generated

Manuscript received August 6, 2010; accepted November 22, 2010.

The authors are with the Electrical Systems and Optics Research Division, University of Nottingham, Nottingham, UK (e-mail: xuesheng.chen@nottingham.ac.uk).

Digital Object Identifier 10.1109/TUFFC.2011.1824

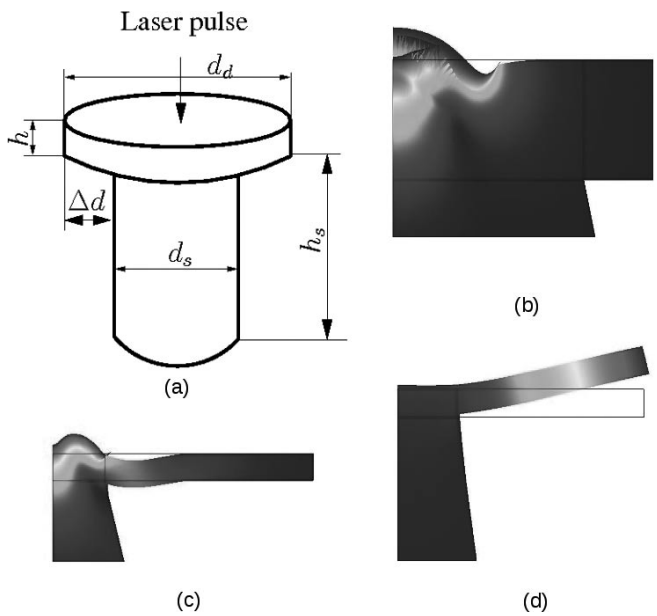

Fig. 1. (a) Schematic design of the geometry of an optical transducer. It is a microdisk with diameter d_{d} and thickness h, seated on a microstem with a diameter d_{s} and a length h_{s}. When a laser pulse is incident on the center of the disk, a resonant flapping motion of the disk is activated, coupling a longitudinal wave propagating along the axis of the stem. (b) A surface wave is actuated first at the disk center by a laser pulse. (c) The surface wave turns into an antisymmetric Lamb wave as it passes the flange root of the disk. (d) Reflections of the Lamb wave between the disk edge and root turn the Lamb wave into a flapping motion of the disk.

ultrasound is broadband [14]–[16]. When a laser pulse is incident on a microdisk [Fig. 1(a)], it produces localized temperature differences and stresses which excite the vibrational modes of the entire structure because of its small size. In the case in which laser light is well focused at the center of the disk, a surface wave with a circular wavefront is actuated first [see Fig. 1(b)]. As this surface wave propagates toward the edge of the disk, it turns into an antisymmetric Lamb wave at the disk root [see Fig. 1(c)] because of the small thickness of the disk. Next, reflections of the Lamb wave between the disk edge and the disk root begin because of the small step length Δd and soon turn the Lamb wave into a resonant flapping motion of the disk [Fig. 1(d)]. If the laser light is not well focused, the Lamb wave may be directly actuated within the flange part of the disk, without the surface wave actuation and propagation.

The disk structure is a resonator and the resonance determines the frequency of the transducer. The modes activated by a laser pulse tend to be dominated by one of the natural resonances of the disk, referred to as the main frequency or mode of the transducer; this mode tunes the vibration of the disk. Usually it is the first resonance that is dominantly actuated if the disk is 2-D and axisymmetric. Depending on the parameter $\Delta d/h$, the material, and the optical actuation, other modes—higher or lower than the main mode of the transducer—may be actuated at the same time, particularly for the case in which the transducer is nonaxisymmetric. It is necessary to point out that although theoretically a transducer can be simplified to be 2-D axisymmetric, an actual transducer is usually nonaxisymmetric because of material anisotropy, fabrication errors, or the optical alignment; the actual main frequency can be a higher-order resonance.

B. Actuation of the Narrowband Longitudinal Wave

For an axisymmetric 2-D disk with a suitable $\Delta d/h$, with a laser pulse incident on the disk center, the actuated modes are dominated by the first resonance of the disk, resulting in a nearly sinusoidal resonant flapping motion of the disk. Because the disk is elastically supported by the solid stem, this resonant flapping motion couples a surface wave traveling along the surface of the stem. The surface wave consists of a transverse wave and a longitudinal wave [17]. Because of the structural axisymmetry, the phase of the transverse wave is axisymmetric with respect to the cross section of the stem. Thus, the coupled transverse wave is canceled out because of the small diameter of the stem. However, the coupled longitudinal wave is in-phase around the stem cross section. Therefore, the coupling of the disk resonant flapping vibration leaves an enhanced longitudinal wave, traveling along the axis of the stem, with a bandwidth the same as that of the disk resonant motion. Because the bandwidth is defined by the resonant motion of the disk, it should be narrower than normal laser generation of ultrasound reported in the literature [9]–[12].

From this working principle, two conditions are important for a successful transducer design: only one mode is dominantly actuated and the phase of the mode should be the same around the circumference of the disk. The first condition ensures that the generated wave is narrowband; the second enables that most of the kinetic energy induced by the absorbed optical energy is tuned into this narrowband wave. Therefore, it is a key step to design a disk resonator for which, for a given laser pulse, only one mode is dominantly actuated and other modes should be minimized. In a case in which the disk of the transducer is not 2-D, or the transducer is not axisymmetric, the resonant mode may be non-axisymmetric with a phase changeable around the disk circumference. In this case, the coupled transverse wave cannot be completely canceled and the longitudinal wave may be partially canceled. This reduces the efficiency and decreases the SNR of the ultrasound system, or widens the corresponding bandwidth; as a consequence, the amplitude of the generated ultrasound is reduced.

III. Finite Element Simulation of the Transducer

To design an optical transducer with maximized output amplitude, the finite element (FE) method was applied to simulate the ultrasound that is generated by the transducer, to find the optimum conditions to achieve ultrasound

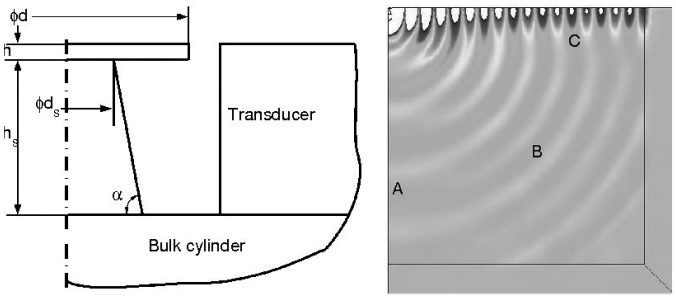

Fig. 2. (left) Geometry of the FE model for an optical transducer. $\alpha = 82°$ for all designed transducers and other dimensions are shown in Table I. (right) FE simulated narrowband surface wave, longitudinal wave, and shear wave generated by the MEMS transducer. The generated waves are distributed in three different areas: A = longitudinal wave, B = shear wave, and C = surface wave.

with the narrowest bandwidth and the highest amplitude. The transducer is assumed to be axisymmetric, in terms of both geometry and physical properties of the polysilicon material. Fig. 2(left) shows the geometry of the FE model for a transducer design; it is bonded to a cylinder with much larger dimensions. We built the model to simulate the propagation of the laser ultrasound from the transducer into the cylinder material.

For this thermomechanically coupled axisymmetric FE model, the absorbed optical power density, q, of a laser pulse incident on the disk surface of the transducer at $r = 0$, as a thermal boundary condition, can be expressed as [18]

$$q = \beta q_0 \exp\left(-\frac{r^2}{r_0^2}\right)\frac{t}{t_0}\exp\left(-\frac{t}{t_0}\right), \tag{1}$$

where q_0 is the maximum laser power density, β is the optical absorption coefficient of the surface of the disk material, r_0 is the radius of the laser beam spot, t_0 is the rise time of the laser pulse, and r and t are the transient location and time. In our lab, a Q-switched Nd:YAG laser with a maximum power of 300 mW at 10 kHz, and a rise time $t_0 = 5$ ns is used. Although the absorption coefficient β is usually an unknown constant, the value of βq_0 only affects the simulated wave amplitude; the waveform, as a function of time and location, is irrelevant to β. We can assume β is a constant, for example, of 5%.

Fig. 2(right) shows a typical result of FE simulated waves for a 2-MHz transducer with stem diameter $d_s = 100$ μm, in which the transducer is located in the upper-left corner of the diagram, nearly invisible because of its small size. Eq. (1) was set by $t_0 = 5$ ns and $r_0 = 50$ μm. From the diagram, it can be seen that a longitudinal wave is, as expected, generated in the area labeled A just below the bottom of the transducer stem. In area B, a shear wave is generated, and in area C—near the surface of the wafer—a strong surface wave is produced, propagating away from the center of the transducer.

Fig. 3 shows the FE-simulated waveforms and the corresponding Fourier transforms from the center of the stem

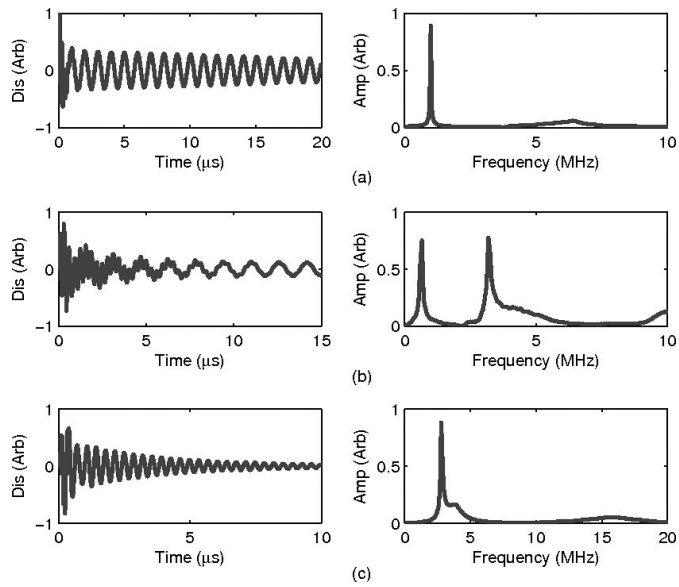

Fig. 3. FE simulated longitudinal waves at the center of the stem bottom surface, and the corresponding Fourier transformations, for (a) a 1-MHz transducer with $\Delta d/h = 6.24$, (b) a 0.667-MHz transducer with $\Delta d/h = 10$, and (c) a 3-MHz transducer with $\Delta d/h = 3.44$.

bottom surface of each transducer. Fig. 3(a) shows the simulated trace of a 1-MHz transducer with $\Delta d/h = 6.24$ and $d_s = 100$ μm, Fig. 3(b) illustrates the ultrasound of a 0.667-MHz transducer with $\Delta d/h = 10$ and $d_s = 100$ μm, and Fig. 3(c) demonstrates the waveform of a 3-MHz transducer with $\Delta d/h = 3.44$ and $d_s = 150$ μm. It can be seen that ultrasound with the expected frequency was generated; however, waves with higher frequencies were also generated, depending on the $\Delta d/h$ parameter. For $h = 25$ μm, the first resonance and the second mode are effectively activated for the transducer with $\Delta d/h = 10$ [Fig. 3(b)], whereas for the case where $\Delta d/h = 6.24$ [Fig. 3(a)] the amplitude of the higher frequencies is much lower. This shows that a high value of $\Delta d/h$ may cause the higher axisymmetrical modes of the disk to be actuated. However, too low a value of $\Delta d/h$ is also not good. This is shown in Fig. 3(c) for the 3-MHz transducer with $\Delta d/h = 3.44$; the bandwidth is obviously wider than that with $\Delta d/h = 6.24$. This suggests that for a given disk thickness h, there is an optimum value of $\Delta d/h$ by which ultrasound with the narrowest bandwidth and highest amplitude can be achieved, and accordingly the corresponding frequency can be defined by the optimum $\Delta d/h$. The FE simulation shows that for a polysilicon disk with thickness of $h = 25$ μm, the corresponding defined frequency is around 1 MHz [Fig. 3(a)] with an optimum value of $\Delta d/h$ around 6.

IV. Design and Fabrication of the Transducer

The purpose of the design process is to define the optimum geometry of a transducer of a required frequency to achieve the ultrasound with the highest amplitude. The

TABLE I. FREQUENCIES AND DIMENSIONS OF THE DESIGNED MEMS TRANSDUCERS.

f (MHz)	d_d (μm)	D_s (μm)	h (μm)	h_s (μm)
1	412	100	25	401
	462	150		
	512	200		
2	310	100		
	360	150		
	410	200		
3	272	100		
	322	150		
	372	200		

geometries of the designed MEMS transducers, with frequencies of 1, 2, and 3 MHz, are shown in Table I. The 1-MHz transducers were designed as being optimal and the 2- and 3-MHz transducers were designed for comparison. As a typical two-mask-level MEMS device, the transducer design is strongly influenced by the fabrication process. The transducers were fabricated by a standard MEMS process, silicon-on-insulator micromachining, by MEMSCAP (http://www.memscap.com). A silicon-on-insulator (SOI) wafer with primary flat direction (100) was used as the basic material for the transducer design and fabrication. The design layer thickness of the wafer is 25 μm, which defines the disk thickness, h, of the transducer. Fig. 4(a) shows the top view of the designed transducers. The 3-D structure for a 3-MHz transducer is shown by Fig. 4(b). As can be seen from the image, the fabricated stem is not a solid cylinder as shown in Fig. 1(a), but a truncated cone because of the restrictions of the design rules of the fabrication process. In this case, the stem diameter means the diameter of cross-section of the stem at the lower surface of the disk. In addition, four spokes are used to support the transducer; each spoke is only connected to the stem at the bottom location; the upper part of each spoke and the disk are completely free from each other.

Two deep reactive ion etching processes were used to fabricate the transducer. Details of the fabrication process can be found on the website of MEMSCAP [19]. Figs. 4(c)–4(f) are images of fabricated transducers under a microscope, where Fig. 4(c) shows the top view of two 1-MHz transducers with $d_s = 100$ and 150 μm and Fig. 4(e) shows the top view of two 3-MHz transducers with the same d_s. Figs. 4(d) and (f) demonstrate the corresponding back side images of the transducers, where the blurred part in each photo is the image of the disk for each transducer viewed from the back side of the wafer.

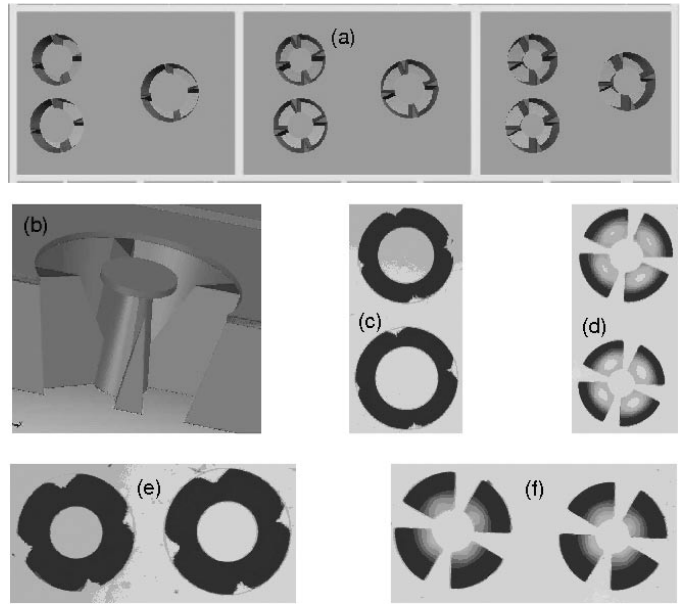

Fig. 4. Geometry design of the MEMS transducers. (a) Image of top view of the designed 1-MHz (left), 2-MHz (middle), and 3-MHz (right) transducers with stem diameters of 100, 150, and 200 μm, respectively. (b) 3-D structure of a 3-MHz transducer. (c) and (d) Front and back images of the 1-MHz transducers with different stem diameters under a microscope. (e) and (f) Similar images of 3-MHz transducers.

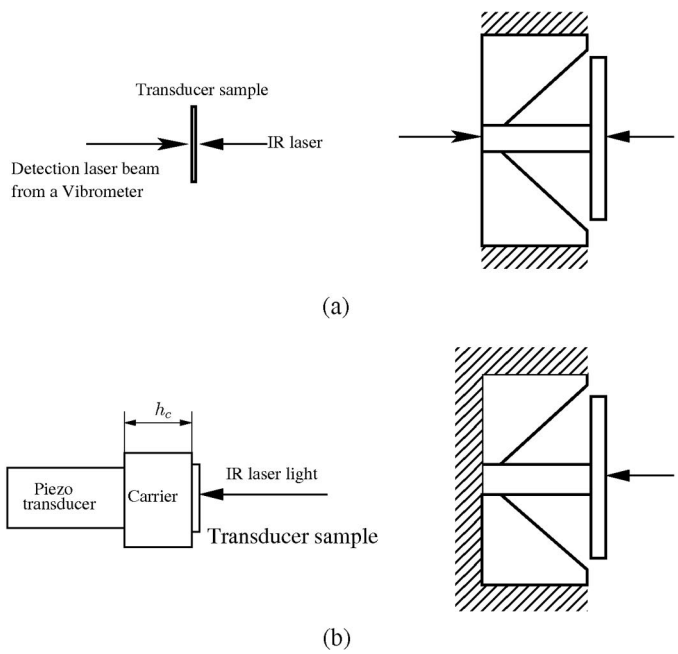

Fig. 5. (a) Experimental configuration for c-scans by using a laser vibrometer. Measurement laser light from the vibrometer scans the bottom of each transducer. (b) Measuring the optically generated ultrasound by using a piezoelectric transducer.

V. EXPERIMENTAL STUDY OF THE TRANSDUCERS

A. Test Configurations and Experimental Results

To see if the designed and fabricated transducers can be applied to optically generate ultrasound with a high amplitude as expected, two systems were configured, as shown in Fig. 5, to conduct experimental studies with these fabricated transducers. Fig. 5(a, left) shows a c-scan system using a laser vibrometer. The head of the vibrometer was amounted on an x-y stage (not shown). A sample of fabricated transducers was held vertically by a stiff frame on the test table. Light pulses produced by the Q-switched Nd:YAG laser were used to actuate the transducers. While

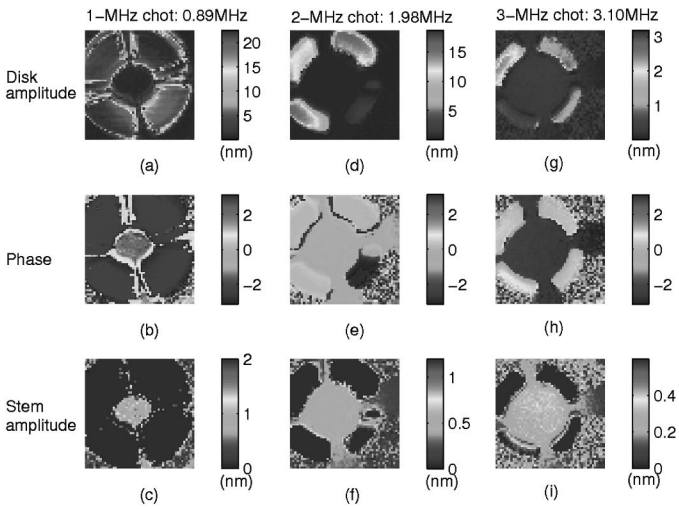

Fig. 6. C-scan images showing the laser-actuated modal shapes of the MEMS transducers at different resonances. (a) Disk amplitude of a 1-MHz transducer at a resonance of 0.89 MHz, (b) the corresponding phase, and (c) the stem surface amplitude. (d) Disk amplitude of a 2-MHz transducer at resonance of 1.98 MHz, (e) the corresponding phase, and (f) the stem surface amplitude. (g) Disk amplitude of a 3-MHz transducer at frequency of 3.1 MHz, (h) the corresponding phase, and (i) the stem surface amplitude. All images were scanned in an area of 400 × 400 μm.

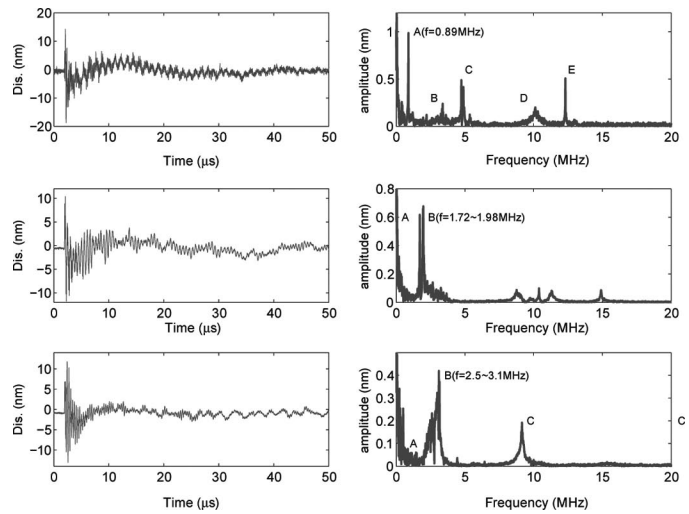

Fig. 7. Ultrasound generated by the MEMS transducers, detected by the laser vibrometer in Fig. 5(a). The left diagrams show the average displacement at stem surface and the right diagrams show the corresponding Fourier transformations for (top) the 1-MHz transducer, (middle) the 2-MHz transducer, and (bottom) the 3-MHz transducer.

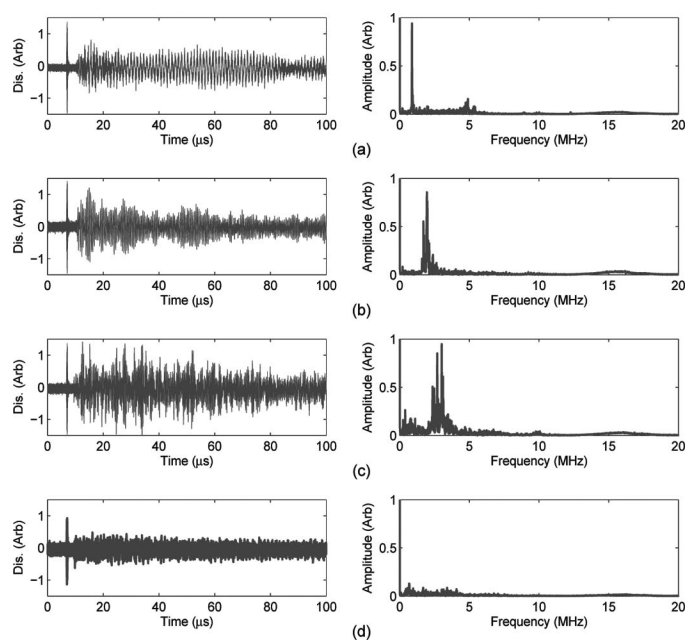

Fig. 8. Ultrasound generated by the MEMS transducers and detected by the piezoelectric transducer in Fig. 5(b). The left diagrams show the traces and the right graphs show the corresponding Fourier transforms for (a) the 1-MHz transducer with $h_c = 15$ mm, (b) the 2-MHz transducer with $h_c = 15$ mm, (c) the 3-MHz transducer with $h_c = 10$ mm, and (d) a normal thermoelastic generation with $h_c = 15$ mm.

the laser pulse is suitably focused and incident on the center of the disk of a transducer on the sample, a flapping motion of the disk and a longitudinal wave along the stem are expected to be generated, leading to a translational motion of the stem bottom surface. By using the detection laser light from the vibrometer, motion of the disk and the stem bottom surface can be scanned from the back of each transducer. In this configuration, each transducer is only supported by four spokes [refer to Fig. 4(b)], and the bottom surfaces of the stem and each spoke are mechanically free, as shown by right part of Fig. 5(a), permitting vibration detection using the vibrometer.

In the configuration of Fig. 5(b), the optical transducer sample is attached to the surface of a carrier with thickness h_c. The carrier is bonded to the surface of a piezoelectric transducer. When a laser pulse is incident on the disk of a transducer on the sample, the generated ultrasound travels through the carrier and can be sensed by the piezoelectric transducer. We used a 5-MHz Olympus V609-SB 5.0/0.5 Videoscan piezoelectric transducer (Olympus NDT, Kennewick, WA) with a bandwidth of 110%. In this configuration, the stem is not only supported by the four spokes [refer to Fig. 4(b)], but also bonded to the surface of the carrier, so that the bottom surfaces of the stem and each spoke are elastically fixed, as shown by the right part of Fig. 5(b).

Fig. 6 provides c-scans, showing modal shape images for different transducers at different resonances by using the experimental system shown by Fig. 5(a). Fig. 7 shows the ultrasound detected at each stem bottom surface and the corresponding Fourier transforms. Fig. 8 shows the ultrasound detected by the test system shown in Fig. 5(b) with the piezoelectric detection transducer and aluminum carriers with thicknesses of 10 and 15 mm.

B. Discussion

1) 1-MHz Transducer: It can be seen from Fig. 6 that the resonant flapping motion of the disk for each transducer was successfully excited by the incident laser pulse. Figs. 6(a) and 6(b) show the nearly axisymmetrical modal

shape at resonance of 0.89 MHz for a 1-MHz transducer; Fig. 6(a) shows the amplitude out of the disk plane and Fig. 6(b) illustrates the corresponding phase. The displacement of the stem bottom surface is much lower than the 20 nm amplitude of the flange flapping motion. However, the surface has nearly constant phase and amplitude, as shown by Figs. 6(b) and 6(c), suggesting that a longitudinal wave is being generated. It can be shown that when the frequency is slightly different, for instance, from 0.89 to 0.98 MHz, the corresponding phase and amplitude of the stem bottom surface were soon below the noise level. This indicates the generated longitudinal wave has a narrow bandwidth, centered at 0.89 MHz. The ultrasound of the stem bottom surface was averaged, analyzed by Fourier transformation and shown by Fig. 7(top). It can be seen that the generated ultrasound around 0.89 MHz, labeled A, was the strongest, although there are some other signals at different frequencies marked B, C, D, and E. These are assumed to be the signals coupled from the actuated higher modes of the transducer. All modes corresponding to these peaks were obtained and shown to be 3-D, either axisymmetrical or non-axisymmetric.

However, these high-frequency signals were not obviously detected by using the detection system shown by Fig. 5(b) with the piezoelectric transducer and an aluminum carrier with a thickness of $h_c = 15$ mm, as shown by Fig. 8(a); only the narrowband ultrasound around 0.89 MHz was detected. One possible reason is that the mechanical boundary conditions are different for the transducer when the experimental configurations in Figs. 5(a) and 5(b) were applied. It should be noted that the sensitivity of the piezoelectric transducer is higher around 5 MHz than that at 1 MHz, so these higher-order modes would be expected to be detected if they were transmitted to the transducer.

2) 2-MHz Transducer: A similar discussion can be had for the 2-MHz transducer with $d_s = 200$ μm; the scanned images were shown in Figs. 6(d), 6(e), and 6(f), where Figs. 6(d) and 6(f) illustrate the amplitude of the disk to be about 15 nm and the amplitude of the stem bottom surface to be more than 0.5 nm, and Fig. 6(e) shows the corresponding phase. The model shape for the 2-MHz disk is not axisymmetric, probably as a result of a fabrication effect; however, this device still generates a strong signal around 1.98 MHz, as shown by Fig. 7(middle) and Fig. 8(b).

3) 3-MHz Transducer: For the 3-MHz transducer with $d_s = 150$ μm, its mode at 3.1 MHz is shown in Figs. 6(g) and 6(h), and the generated longitudinal wave is shown by Figs. 6(h) and 6(i) for constant phase and amplitude within the stem bottom surface. The corresponding scanned ultrasound and the ultrasound detected by the piezoelectric transducer are shown in Figs. 7(bottom) and Fig. 8(c).

4) Comparison With Normal Thermoelastic Generation: To show the high efficiency of this optical transducer, a comparison between the transducer generation and the normal thermoelastic generation has been shown by Figs. 8(a) and 8(d). Fig. 8(d) shows the ultrasound from normal thermoelastic generation with the same optics using the substrate away from any structure. It can be seen that amplitude of the broadband ultrasound by normal thermoelastic generation is only at the noise level of the narrowband ultrasound generated by the MEMS transducer; the amplitude of the generated narrowband ultrasound is at least 5 times higher than that of the normal thermoelastic generation (Figs. 8(a) and 8(d) are on the same scale). More important is that the SNR of the narrowband ultrasound is much higher than that of the broadband ultrasound generated. It is an interesting fact that the amplitude achieved by the MEMS transducer was difficult to reach by normal optical generation, even with the input optical power in the ablation range. This is an advantage of this optical transducer over a simple absorption layer.

For the resonant flapping motion of a disk, it is not necessary for the laser light to be well focused; a laser spot matching the disk can increase the laser power while the power density still remains within thermoelastic regimen. Thus, pulsed light from a laser with relatively higher power can be applied to this transducer. One hopeful improvement of the transducer is to combine this with the technique presented in [6], in which a highly absorbing layer deposited onto the disk surface of the MEMS transducer for use with a less powerful laser. For high-frequency narrowband ultrasound, a finer disk array transducer can perhaps be designed.

VI. Conclusions

The dynamic behavior of a microdisk actuated by a laser pulse is completely different from that of a normal sample; one of the disk modes is dominant among all the actuated modes, resulting in a resonant flapping motion of the disk and further coupling a narrowband ultrasound. It is important to design a 2-D axisymmetric disk with an optimum ratio of $\Delta d/h$. Based on this, optical MEMS generation transducers were designed and fabricated. FE simulation and experimental study have shown that these transducers can be applied to optically generate narrowband ultrasound—surface wave, shear wave and longitudinal wave—with high efficiency, high amplitude/SNR, and narrow bandwidth; compared with normal thermoelastic generation, ultrasound with at least 5 times higher amplitude can be achieved by a suitably designed optical transducer. Only a single laser source with a simple optical arrangement is required to use this transducer.

References

[1] S. J. Davies, C. Edwards, G. S. Taylor, and S. B. Palmer, "Laser-generated ultrasound: Its properties, mechanisms and multifarious applications," *J. Phys. D*, vol. 26, no. 3, pp. 329–348, 1993.

[2] A. S. Murfin, R A J. Soden, D. Hatrick, and R. J. Dewhurst, "Laser-ultrasound detection systems: A comparative study with Rayleigh waves," *Meas. Sci. Technol.*, vol. 11, no. 8, pp. 1208–1219, 2000.

[3] K. C. Baldwin, T. P. Berndt, and M. J. Ehrlich, "Narrowband laser generation/air-coupled detection: Ultrasonic system for on-line process control of composites," *Ultrasonics*, vol. 37, no. 5, pp. 329–334, 1999.

[4] X. Chen, T. Stratoudaki, S. D. Sharples, and M. Clark, "Design and experimental study of microcantilever ultrasonic detection transducers," *IEEE Trans. Ultrason. Ferroelectr. Freq. Control*, vol. 56, no. 12, pp. 2722–2732, 2009.

[5] D. Karabacak and T. Kouha, "Optical knife-edge technique for nanomechanical displacement detection," *Appl. Phys. Lett.*, vol. 88, no. 19, art. no. 193122, 2006.

[6] E. Biagi, F. Margheri, and D. Menichelli, "Efficient laser-ultrasound generation by using heavily absorbing films as targets," *IEEE Trans. Ultrason. Ferroelectr. Freq. Control*, vol. 48, no. 6, pp. 1669–1680, Nov. 2001.

[7] I. Arias and J. D. Achenbach, "Thermoelastic generation of ultrasound by line-focused laser irradiation," *Int. J. Solids Struct.*, vol. 40, no. 25, pp. 6917–6935, 2003.

[8] T. Stratoudaki, J. A. Hernandez, M. Clark, and M. G. Somekh, "Cheap optical transducers (CHOTs) for narrowband ultrasonic applications," *Meas. Sci. Technol.*, vol. 18, no. 3, pp. 843–851, 2007.

[9] J. W. Wagner, J. B. Deaton, and J. B. Spicer, "Generation of ultrasound by repetitively Q-switching a pulsed Nd:YAG laser," *Appl. Opt.*, vol. 27, no. 22, pp. 4696–4700, 1988.

[10] J. B. Deaton Jr., A. D. W. McKie, J. B. Spicer, and J. W. Wagner, "Generation of narrowband ultrasound with a long cavity mode-locked Nd:YAG laser," *Appl. Phys. Lett.*, vol. 56, no. 24, pp. 2390–2392, 1990.

[11] Y. H. Berthelot and J. Jarzynski, "Directional laser generation and detection of ultrasound with arrays of optical fibers," *J. Nondestr. Eval.*, vol. 9, no. 4, pp. 271–277, 1990.

[12] J. W. Wagner, A. D. W. McKie, J. B. Spicer, and J. B. Deaton Jr., "Modulated laser array sources for generation of narrowband and directed ultrasound," *J. Nondestr. Eval.*, vol. 9, no. 4, pp. 263–270, 1990.

[13] A. Giannoula and R. S. Cobbold, "Narrowband shear wave generation by a finite-amplitude radiation force: The fundamental component," *IEEE Trans. Ultrason. Ferroelectr. Freq. Control*, vol. 55, no. 2, pp. 343–358, 2008.

[14] L. R. F. Rose, "Point-source representation for laser-generated ultrasound," *J. Acoust. Soc. Am.*, vol. 75, no. 3, pp. 723–731, 1984.

[15] H. D. Hurley and J. B. Spicer, "Point-source representation for laser-generated ultrasound in an elastic, transversely isotropic half-space," *J. Appl. Phys.*, vol. 86, no. 6, pp. 3423–3427, 1999.

[16] Y. Pan, M. Perton, B. Audoin, and C. Rossignol, "Acoustic waves generated by a laser point pulse in a transversely isotropic cylinder," *J. Acoust. Soc. Am.*, vol. 119, no. 1, pp. 243–250, 2006.

[17] J. P. Shull, *Nondestructive Evaluation, Theory, Techniques and Applications*. Boca Raton, FL: CRC Press, 2002.

[18] B. Xu, Z. Shen, X. Ni, and J. Lu, "Numerical simulation of laser-generated ultrasound by the finite element method," *J. Appl. Phys.*, vol. 95, no. 4, pp. 2116–2122, 2004.

[19] MEMSCAP SA, (2011, Jan.) MUMPs. [Online]. Available: http://www.memscap.com/en_mumps.html

Xuesheng Chen obtained his Ph.D. in precision cold forging in 2002 at the University of Strathclyde in the UK. He is now a research fellow in the Electrical Systems and Optics Research Division, working on noncontact ultrasound detection transducers and laser ultrasound generation transducers.

Theodosia Stratoudaki obtained her Ph.D. in physics in 2003 from the University of Warwick. She joined the Applied Optics Group at the University of Nottingham in 2004 as a research fellow. Her research interests are in ultrasonics and laser applications including nonlinear ultrasonics. Recently she has been designing and developing novel optical transducers for applications in nondestructive testing of materials.

Steve D. Sharples obtained his Ph.D. in applied optics in 2003 from the University of Nottingham, UK. He is a senior research fellow in the Applied Optics Group, within the Electrical Systems and Optics Research Division. He has worked on laser ultrasound systems for more than ten years, researching novel excitation and detection techniques enabling faster imaging and interesting contrast mechanisms, with applications in nondestructive evaluation and materials characterization.

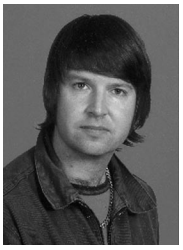

Matthew Clark was born in Norwich, UK, in 1968. His first degree was in physics from Manchester University, UK, where he graduated in 1990. He went to Imperial College, London as a research assistant and stayed to complete his Ph.D. in optics in the Physics Department in 1997. He has worked in the School of Electrical and Electronic Engineering, University of Nottingham since 1996. He was an EPSRC Advanced research fellow from 2000 to 2005 and currently holds an EPSRC Challenging Engineering award.